3

Growth of Nanowire and Nanobelt Based Oxides by Thermal Oxidation with Gallium

Qing Yang[1], Takahito Yasuda[1], Hitonori Kukino[1],
Miyoko Tanaka[2] and Hirokazu Tatsuoka[1]
[1]*Shizuoka University*
[2]*National Institute for Materials Science*
Japan

1. Introduction

Quasi-one-dimensional nanostructure based oxides, such as nanowires and nanobelts, have attracted much attention in recent years, which exhibit unusual optical, electronic or mechanical properties as compared to those of bulk materials, due to the significant surface related defects originating from the high surface to volume ratios. In addition, some important advantages such as good high temperature stability, oxidation resistance and stable electric properties, demonstrate their potential basic building blocks for new classes of environmentally conscious electronics. Much effort has been made to develop nanoscale optical and electronic devices for the generation of renewable energy using the nanowire and nanobelt based oxides. As a simple and scalable growth method, the oxidation behavior of metals has been typically conducted on the nanostructure growth of metal oxides over several decades (Chen et al., 2008; Gu et al., 2002; Jiang et al., 2002; Ren et al., 2007; Takagi, 1957; Yu et al., 2005; Yu et al., 2006). On the other hand, Pan et al. reported the SiO_x nanowire growth using gallium (Pan et al., 2002; 2003; 2005). In addition, a variety of oxide nanostructures have been synthesized by the thermal oxidation of silicide alloys with gallium (Ogino et al., 2007). In this paper, we report a variety of nanowire and nanobelt based oxides (ZnO, α-Fe_2O_3, β-Ga_2O_3) grown by the thermal oxidation with gallium in air.

2. Growth & characterization

The oxide nanostructures were synthesized by the thermal oxidation of the source substrates with gallium in air. Gallium was melted around 35~40 °C, then manually applied to the substrates using a stick. The substrates with gallium were loaded into a quartz tube which is open to the air. The oxide nanostructure growth was performed by exposure of the substrates with gallium to the air, and the oxide nanostructures were grown at elevated temperatures for several hours.

The as-grown oxide nanostructures were characterized by scanning electron microscopy (SEM), transmission electron microscopy (TEM) with selected area electron diffraction (SAED) and high-resolution transmission electron microscopy (HRTEM). The compositional analysis was made using energy dispersive X-ray spectroscopy (EDS).

Source: Nanowires Science and Technology, Book edited by: Nicoleta Lupu,
ISBN 978-953-7619-89-3, pp. 402, February 2010, INTECH, Croatia, downloaded from SCIYO.COM

3. Oxide nanowires & nanobelts

3.1 ZnO

ZnO is well known as one of the most promising wide band-gap semiconductor materials, and the ZnO quasi-one-dimensional nanostructures have attracted tremendous attention for its potential applications in nanoscale electronics and optoelectronics (Lu et al., 2006). ZnS has been adopted as a buffer or source material for the growth of various ZnO crystals. ZnO nanorods (Wang et al., 2004) and nanowires (Yuan et al., 2003) were grown by the thermal evaporation of ZnS powders; while using ZnS and $Fe(NO_3)_3$, ZnO whiskers were grown (Hu et al., 2001); ZnO nanobelts were formed by the oxidation of a ZnS nanobelt (Li et al., 2004). Miyake et al. reported a simple growth technique of epitaxial ZnO layers using ZnS substrates (Miyake et al., 2000). The growth of ZnO nanostructures is expected when the thermal oxidation with gallium is applied to the ZnO growth using ZnS substrates. In this section, we report the ZnO nanowires and nanobelts grown at temperatures of 700~900 ^{o}C for 5 h in air.

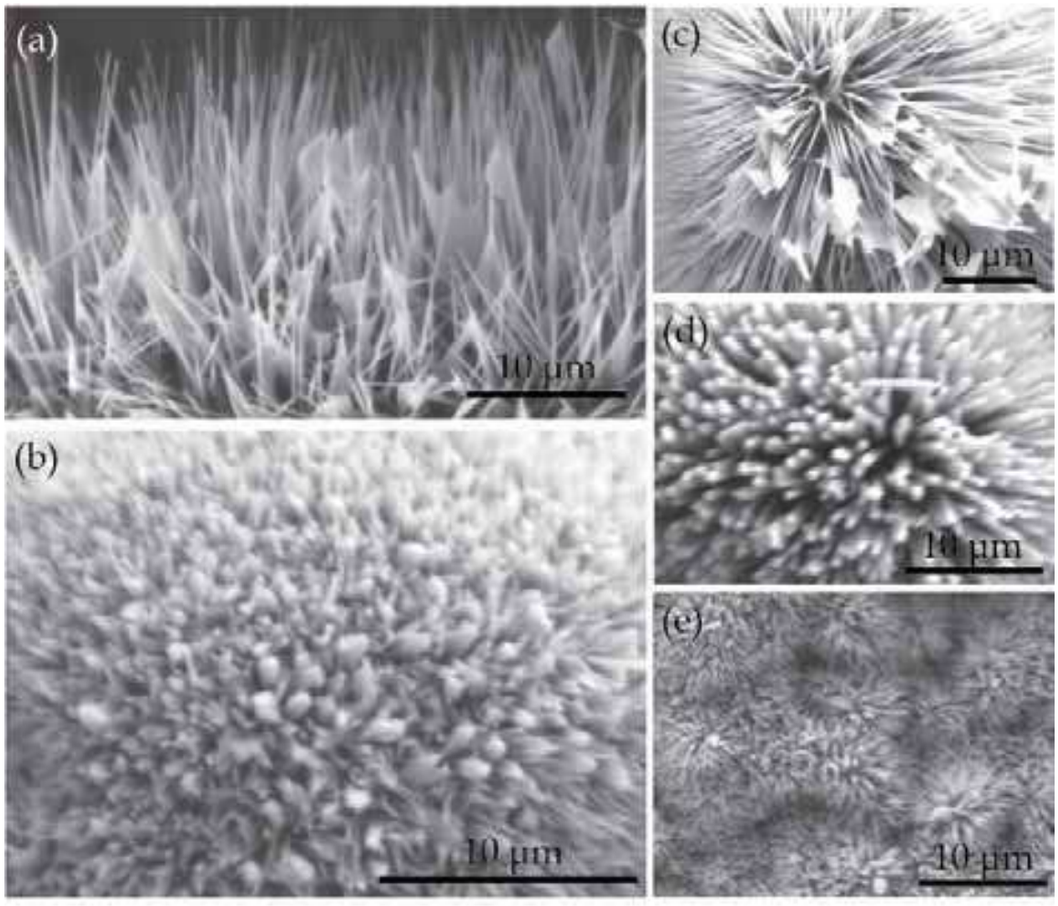

Fig. 1. SEM images of ZnO nanostructures with various morphologies.

Figure 1 shows the SEM images of ZnO nanowires with various morphologies. The diameters of the nanowires vary from 20 to 200 nanometers, and the maximum length extends to tens of micrometers. As shown in Figure 2, the EDS mapping of several nanowires revealed that the observed atomic ratio of Zn/O is near unity, while the impurity atoms of Ga and S are quite few.

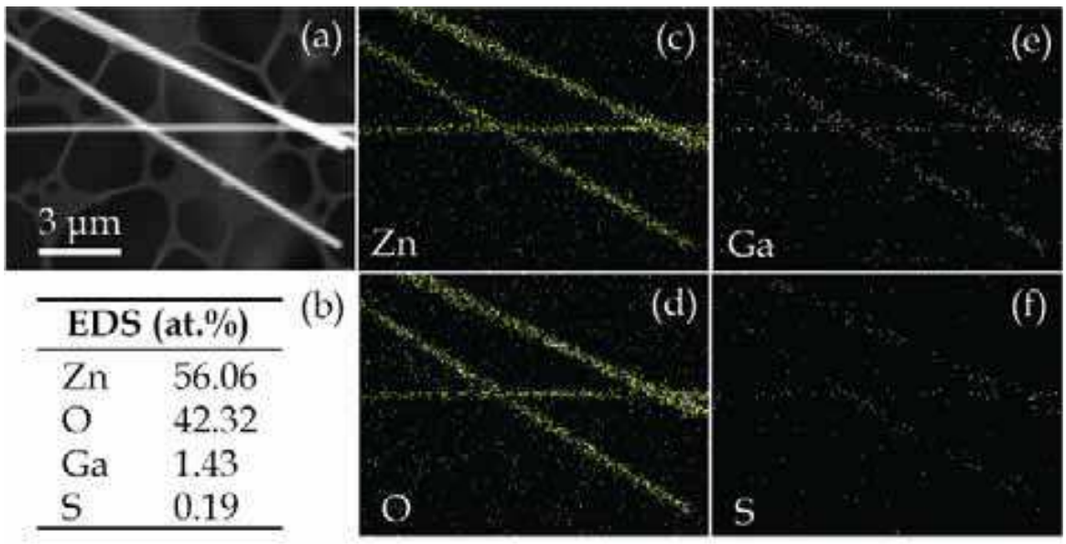

Fig. 2. (a) SEM image of several nanowires and corresponding EDS mapping images of (c) Zn, (d) O, (e) Ga and (f) S. The observed EDS result is shown in (b).

Figures 3 (a) and (b) show the TEM image of a nanowire and corresponding SAED pattern, respectively. The SAED pattern agrees with that of hexagonal ZnO with the incident electron beam parallel to the $[2\bar{1}\bar{1}0]$ direction, and the growth axis of the nanowire is parallel to the [0001] direction.

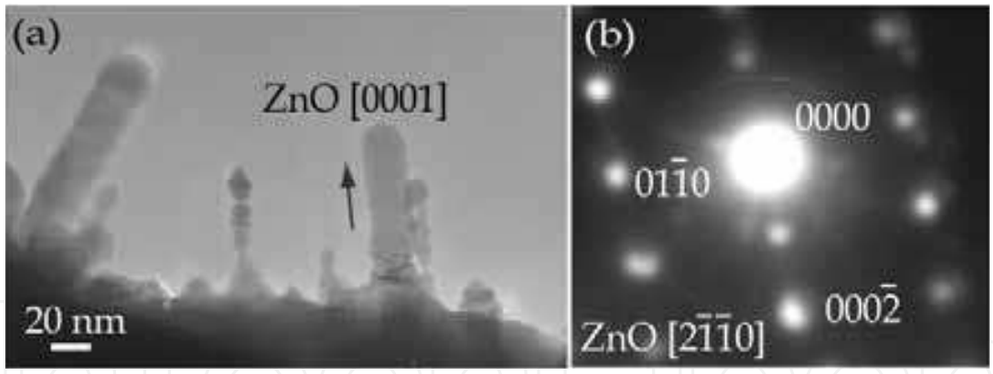

Fig. 3. (a) TEM image and (b) corresponding SAED pattern of one of the nanowires. (Yang et al., 2009)

Figure 4 (a) shows the enlarged TEM image of a nanowire. It was found that the surface of the nanostructure is covered by a thin layer. Figures 4 (b), (c) and (d) show the HRTEM images with SAED patterns in the insets, as marked by B, C, D in Fig. 4 (a), respectively. The plane spacing perpendicular to the growth direction is about 0.26 nm, which is consistent with that of the (0002) planes of the ZnO crystal. Stacking faults lying on the (0001) planes are observed perpendicular to the growth direction, and the streaking SAED pattern in the inset of Fig. 4 (c) is caused by the existence of the stacking faults. As shown in Fig. 4 (d), the average distance of the lattice planes is about 0.43 nm and 0.26 nm. The angle between them is about 75°. The spacing lattice conforms to that of the cubic $ZnGa_2O_4$ crystal (α = 0.8335 nm; JCPDS Card No. 38-1240). The SAED pattern in the inset of Fig. 4 (d) shows that the

$ZnGa_2O_4$ grew along the [010] direction. It was found that the growth direction of the nanowires is ZnO[0001], and which is parallel to $ZnGa_2O_4$[010]. In addition, ZnO$[2\bar{1}\bar{1}0]$ is nearly parallel to $ZnGa_2O_4$[301]. This relationship is roughly equivalent to the relationship as ZnO$(\bar{1}100)$ //$ZnGa_2O_4(101)$ and ZnO$(11\bar{2}0)$ //$ZnGa_2O_4(\bar{1}01)$. In addition, the mismatch of the plane spacings between $d_{ZnO(\bar{1}100)}$ (0.2815 nm) and $d_{ZnGa2O4(202)}$ (0.2947 nm) is about 4.6%, and that of the plane spacings between $d_{ZnO(11\bar{2}0)}$ (0.1625 nm) and $d_{ZnGa2O4(\bar{4}04)}$ (0.1474 nm) about 9.3%. This crystallographic relationship shows a relatively lower lattice mismatch configuration for the ZnO and $ZnGa_2O_4$ couple. It is considered that the observed relationship is provided by the result of the ZnO$(\bar{1}100)$ //$ZnGa_2O_4(101)$ and ZnO$(11\bar{2}0)$ //$ZnGa_2O_4(\bar{1}01)$ crystallographic orientation relationships with a lower lattice mismatch.

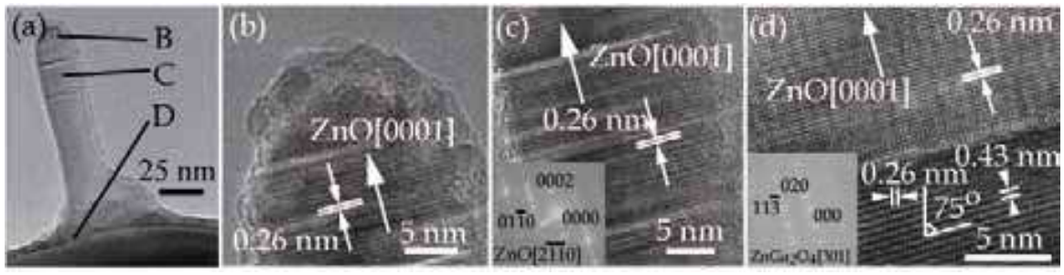

Fig. 4. (a) TEM image of one nanowire, (b,c,d) HRTEM images of the nanowire and corresponding SAED patterns in the insets, as marked by B,C,D in (a). (Yang et al., 2009)

Figures 5 (a) and (c, d, e, f) show the TEM image of the nanowire shown in Fig. 4 (a) and the corresponding Zn, O, Ga and S EDS mapping, respectively. The pictures reveal that the Ga atoms are highly concentrated at the substrate of the nanowire, while the Zn atoms are distributed in both the layer and nanowire. The EDS result reveals that the nanowire mainly contains zinc and oxygen, and the ratio of zinc to oxygen is about 54:45, indicating stoichiometric ZnO. It should be noted that small amounts of Ga or S remain in the ZnO layer. The observed stoichiometry of the substrate region does not strictly agree with that of $ZnGa_2O_4$, which might be caused by the co-existence of other Zn or Ga compounds in deeper regions of the substrate.

Figure 6 shows typical SEM images of the ZnO nano- and micro-belts with a variety of morphological features. Branched (Fig. 6b), stepped (Fig.6c and d) and irregular shaped (Fig. 6d and e) belt-like structures were observed. The morphology of the belt shown in Fig. 6 (e) is quite similar to that reported by (Jian et al., 2006; Zhao et al., 2004), but no droplet exists on the tip of the belt presented here. Meanwhile, several thick belts with cross sectional sides are shown in Fig. 6 (c). In comparison, thin belts were also observed, as shown in Fig. 6 (f, g) and Fig. 8 (d).

Figures 7 (a) and (b, c, d) show the HRTEM images of a stepped nanobelt and the corresponding fast Fourier transform (FFT) patterns, as marked by b, c, d in (a), respectively. As shown in Fig. 7 (a), two domains of the stepped nanobelt are marked by A and B, respectively, and domain A grew from domain B. The plane spacing (shown in the inset of Fig. 7a) parallel to the growth direction of domain A is about 0.15 nm, which corresponds to the $(02\bar{2}0)$ plane of hexagonal ZnO. The FFT patterns reveal that domain A grew along the [0001] direction with wide and narrow surfaces of $\pm(2\bar{1}\bar{1}0)$ and $\pm(0\bar{1}10)$, respectively; while the growth direction of domain B is along the $[0\bar{1}11]$ direction, which is parallel to the

[0001] growth direction of domain A, and both of them have the same flat surfaces of $\pm(2\bar{1}\bar{1}0)$. The domain B growth is quite similar to the nanoplatelet (Ye et al., 2005), which

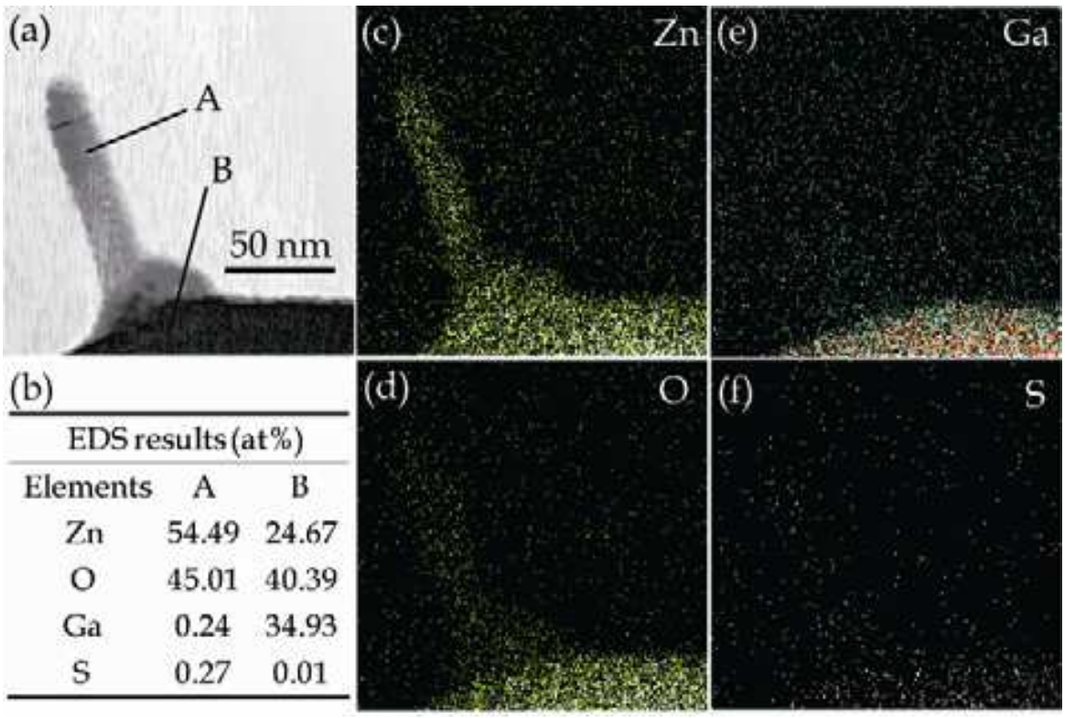

(b)

EDS results (at%)		
Elements	A	B
Zn	54.49	24.67
O	45.01	40.39
Ga	0.24	34.93
S	0.27	0.01

Fig. 5. (a) TEM image of the nanowire shown in Fig. 4 (a), and corresponding EDS mapping images of (c) Zn, (d) O, (e) Ga and (f) S. The observed EDS results are shown in (b). (Yang et al., 2009)

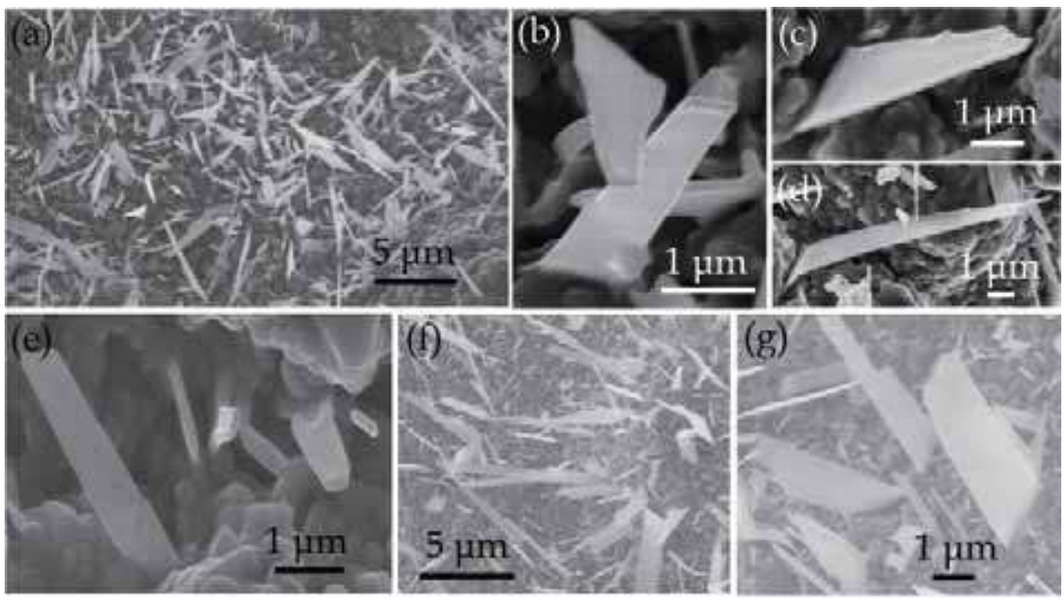

Fig. 6. (a,f) Low magnification SEM images of belt-like structures; typical high magnification SEM images of (b) branched, (c,d) stepped, (d,e) irregular shaped and (f,g) thin belts.

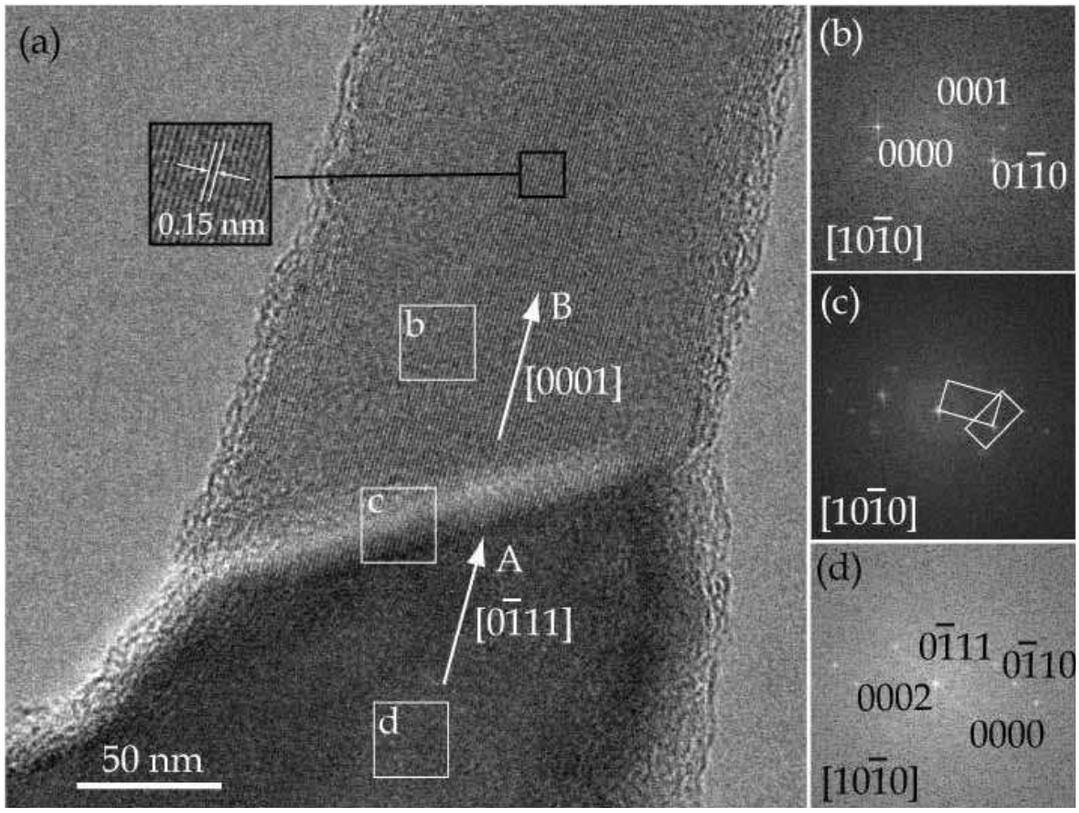

Fig. 7. (a) HRTEM images of a stepped nanobelt and (b,c,d) corresponding FFT patterns.

also grew along the $[01\bar{1}1]$ direction with flat surfaces of $\pm(2\bar{1}\bar{1}0)$. The relationship of the two domains is roughly equivalent to the relationship as $(01\bar{1}0)_A // (10\bar{1}0)_B$ and $(1\bar{1}00)_A // (01\bar{1}\bar{1})_B$. The mismatch of the plane spacings between $d_{(01\bar{1}0)}$ (0.2814 nm) and $d_{(10\bar{1}0)}$ (0.2814 nm) is 0, and that of the plane spacings between $d_{(1\bar{1}00)}$ (0.2814 nm) and $d_{(01\bar{1}\bar{1})}$ (0.2476 nm) is about 12%. This crystallographic relationship shows a relatively lower lattice mismatch configuration for the two domains of the stepped nanobelt. It is considered that the observed relationship is provided by the result of the $(01\bar{1}0)_A // (10\bar{1}0)_B$ and $(1\bar{1}00)_A // (01\bar{1}\bar{1})_B$ crystallographic orientation relationships with a lower lattice mismatch.

Figures 8 (a, b) and (c) show the HRTEM images of a belt and corresponding FFT pattern, respectively. The belt shows two sets of lattice fringes with a spacing of about 0.25 nm and 0.17 nm, normal to each other, corresponding to the (0002) and $(11\bar{2}0)$ planes of hexagonal ZnO. The FFT pattern revealed that the nanobelt grew along the $[11\bar{2}0]$ direction with wide and narrow surfaces of $\pm(1\bar{1}00)$ and $\pm(0001)$, respectively.

Figures 8 (d) and (e) show the TEM image of several nanobelts and corresponding SAED pattern, respectively. The SAED pattern is recorded from the nanobelt as marked by E in Fig. 8 (d), and it can be indexed based on the hexagonal ZnO cell with an electron beam along $[\bar{1}2\bar{1}3]$. It demonstrated that the flat surfaces of the nanobelt is $\pm(\bar{1}2\bar{1}3)$, while the growth directions are perpendicular to $(11\bar{2}\bar{1})$.

ZnO crystals generally grow along the [0001] direction (Fig. 3a, Fig. 4a and Fig. 7a) because of the kinetically fast growth of the (0001) planes for the anisotropic crystal structure (Baxter et al., 2003). Meanwhile, the growth rate of the ZnO crystals along the [0001] direction is

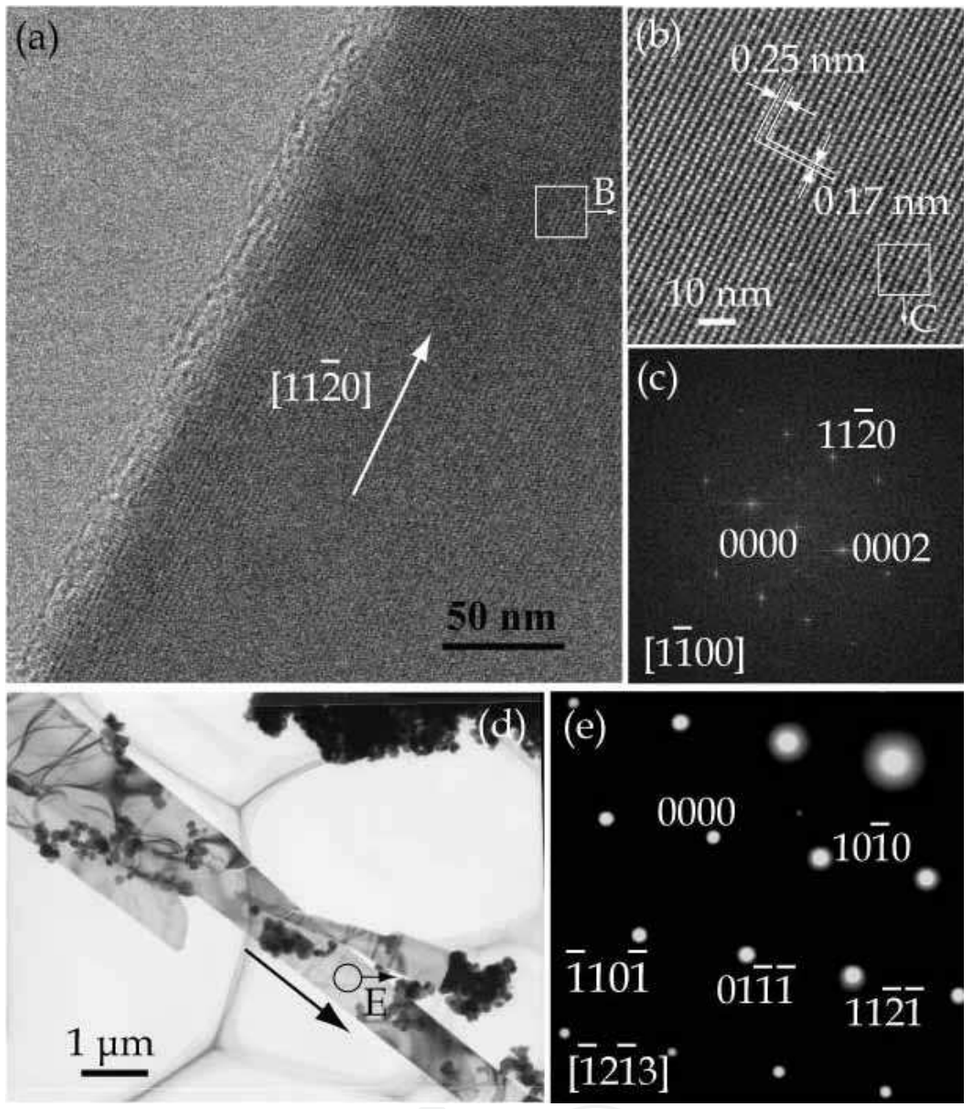

Fig. 8. (a,b) HRTEM images of a nanobelt and (c) corresponding FFT pattern. (d) TEM image of a nanobelt and (e) corresponding SAED pattern.

faster than along the [0$\bar{1}$11] direction (Li et al., 1999). Therefore, the transfer of the growth direction from [0$\bar{1}$11] to [0001] for the stepped nanobelt (Fig. 7a) is possibly determined by the kinetically driven growth and minimization of the surface energy (Ye et al., 2005). ZnO belts growing along the [0001] direction with wide and narrow surfaces of $\pm(2\bar{1}\bar{1}0)$ and $\pm(0\bar{1}10)$ (Fig. 7a) were reported by (Pan et al., 2001; Wang et al., 2004; Ye et al., 2005), and those growing along the [11$\bar{2}$0] direction with wide and narrow surfaces of $\pm(1\bar{1}00)$ and $\pm(0001)$ (Fig. 8a) were reported by (Deng et al., 2005; Li et al., 2004). A few reports described the synthesis of ZnO belts with both morphologies (Ding et al., 2004). However, in the present work, we reported a new type of ZnO nanobelt with flat surfaces of $\pm(\bar{1}2\bar{1}3)$ and growth directions perpendicular to $(11\bar{2}\bar{1})$ (Fig. 8d). Meanwhile, all of the types of ZnO belts were synthesized by the simple growth method, which provides the possibility for the selective growth of ZnO nanostructures by controlling the growth conditions.

The characterizations of the above ZnO nanostructures show that the surface region of the substrate is composed of ZnO or $ZnGa_2O_4$, which indicates that the ZnO nanostructures grew on ZnO or $ZnGa_2O_4$ domains by the oxidization of the surface of ZnS substrate. It has been reported that the selective growth of a particular phase is mainly triggered by a specific interface composition, and is governed by the diffusion flux to the interface (Majni et al., 1981). In this sense, when ZnS is used as the starting material of the growth evolution, O diffusion into ZnS leads to the formation of ZnO near the surface. The enthalpy of formation of ZnO (41.9 kcal/g-atom) (Kubaschewski & Alcock, 1979) is greater than that of ZnS (24.5 kcal/g-atom) (Kubaschewski & Alcock, 1979). The formation of ZnO is thermodynamically favored as compared to that of ZnS. On the other hand, the enthalpy of formation of Ga_2O_3 (51.8 kcal/g-atom) (Kubaschewski & Alcock, 1979) is greater than that of ZnO. If the Ga droplets remained on the ZnS surface, Ga could be oxidized to form Ga_2O_3. It is assumed that Ga atoms are consumed to form $ZnGa_2O_4$, and possibly incorporated into ZnO as impurities.

3.2 α-Fe_2O_3

As one of the oxide semiconductors with a small band-gap of 2.1 eV, α-Fe_2O_3 is the most stable iron oxide under ambient conditions. It is nontoxic, magnetic, corrosion resistant, and

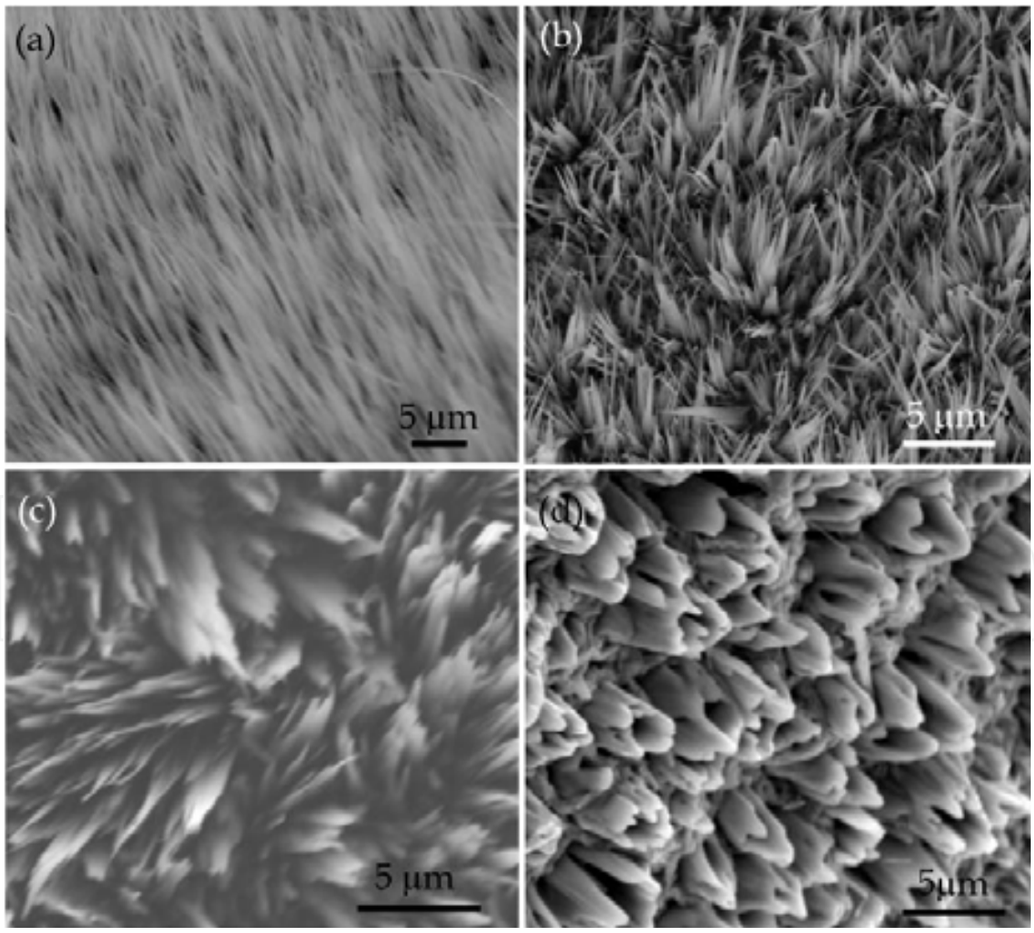

Fig. 9. SEM images of α-Fe_2O_3 nanostructures grown on iron substrates (a,c) without or (b,d) with gallium at (a,b) 700 and (c,d) 800 °C.

has promising applications in photocatalyst (Ohmori et al., 2000), sensor (Liao et al., 2008), magnetic storage media (Kim et al., 2006) and field emission (Yu et al., 2006). To date, various α-Fe_2O_3 nanostructures, including whiskers, nanowires and nanobelts, have been synthesized by the oxidation of iron during a wide temperature range using a hotplate (Yu et al., 2006), reactive oxygen plasma (Cvelbar et al., 2008), oxygen (Takagi, 1957; Wen et al., 2005), ozone (Srivastava et al., 2007), or a gas mixture (Fu et al., 2003; Wang et al., 2005; Xu et al., 2009). In this section, we report the simple synthesis of α-Fe_2O_3 nanowires and nanobelts, via the direct thermal oxidation of iron substrates with or without gallium at temperatures of 600~800 °C for 3 h in air.

Figure 9 shows the SEM images of α-Fe_2O_3 nanostructures grown at temperatures of (a, b) 700 and (c, d) 800 °C by the thermal oxidation of iron substrates (a, c) without or with (b, d) gallium in air. α-Fe_2O_3 nanobelts were grown on iron substrates at 800 °C rather than nanowires grown at 700 °C. On the other hand, α-Fe_2O_3 nanobelts and nanowires were grown on iron substrates with gallium at 700 °C. In addition, it should be pointed out that the morphologies of the two kinds of nanobelts are quite different, and the width of the nanobelts grown without gallium at 800 °C (Fig. 9c) is generally larger than that grown with gallium at 700 °C (Fig. 9b). The detailed structures of the nanowires (Figs. 9a&b) and nanobelts (Figs. 9b&c) were characterized by transmission electron microscopy, which are shown in Figures 10-12.

The TEM image and corresponding SAED pattern of one of the nanowires, grown by the thermal oxidation of iron substrates at 700 °C (Fig. 9a), are shown in Figures 10 (a) and (b), respectively. As shown in Fig. 10 (b), the SAED pattern is composed of two sets of diffraction patterns with zone axis parallel to the [001] and $[\bar{1}11]$ directions, respectively, as marked by the solid lines.

It is indicated that the nanowire is composed of at least two overlapped grains to form a bicrystal structure, and the two overlapped grains share the same growth direction along the [110]. Figure 10 (c) shows an enlarged TEM image of the area marked by circle C in Fig. 10 (a), and the crystal boundary is clearly seen. Figure 10 (d) shows the TEM image of the rectangular enclosed area of the right-side crystal in Fig. 10 (c), the fringe spacing along the growth direction is about 0.252 nm, which corresponds to the interplanar spacing of the (110) planes of α-Fe2O3 (JCPDS Card No. 71-5088), and the corresponding FFT pattern with the $[\bar{1}11]$ zone axis is shown in Figure 10 (e), which confirms the growth direction along [110]. In addition, as shown in Fig. 10 (b), several additional weak diffraction spots as marked by the arrows are observed, which belong to the diffraction patterns with zone axis parallel to the $[\bar{1}11]$ direction, as marked by the dotted lines. It is considered that the diffracted beam travelling through the grain viewed along the [001] direction is re-diffracted when it passes into the other grain viewed along the $[\bar{1}11]$ direction. The observed weak diffraction pattern should be the double diffraction pattern, which occurs at the interface between the thin grains. In addition, few similar double diffraction spots are also observed in the SAED patterns of the nanobelts characterized below.

Figure 11 shows the TEM images of the nanostructures grown by the thermal oxidation of iron substrates with gallium at 700 °C (Fig. 9b). The TEM image containing nanobelts and nanowires is shown in Figure 11 (a). Figure 11 (b) shows the TEM image of a nanobelt with the corresponding SAED pattern in the inset. Figure 11 (c) shows the TEM image of a nanowire, and an enlarged TEM image of the tip part is shown in the left-lower inset with the corresponding SAED pattern shown in the right-upper inset. The nanowire, with a

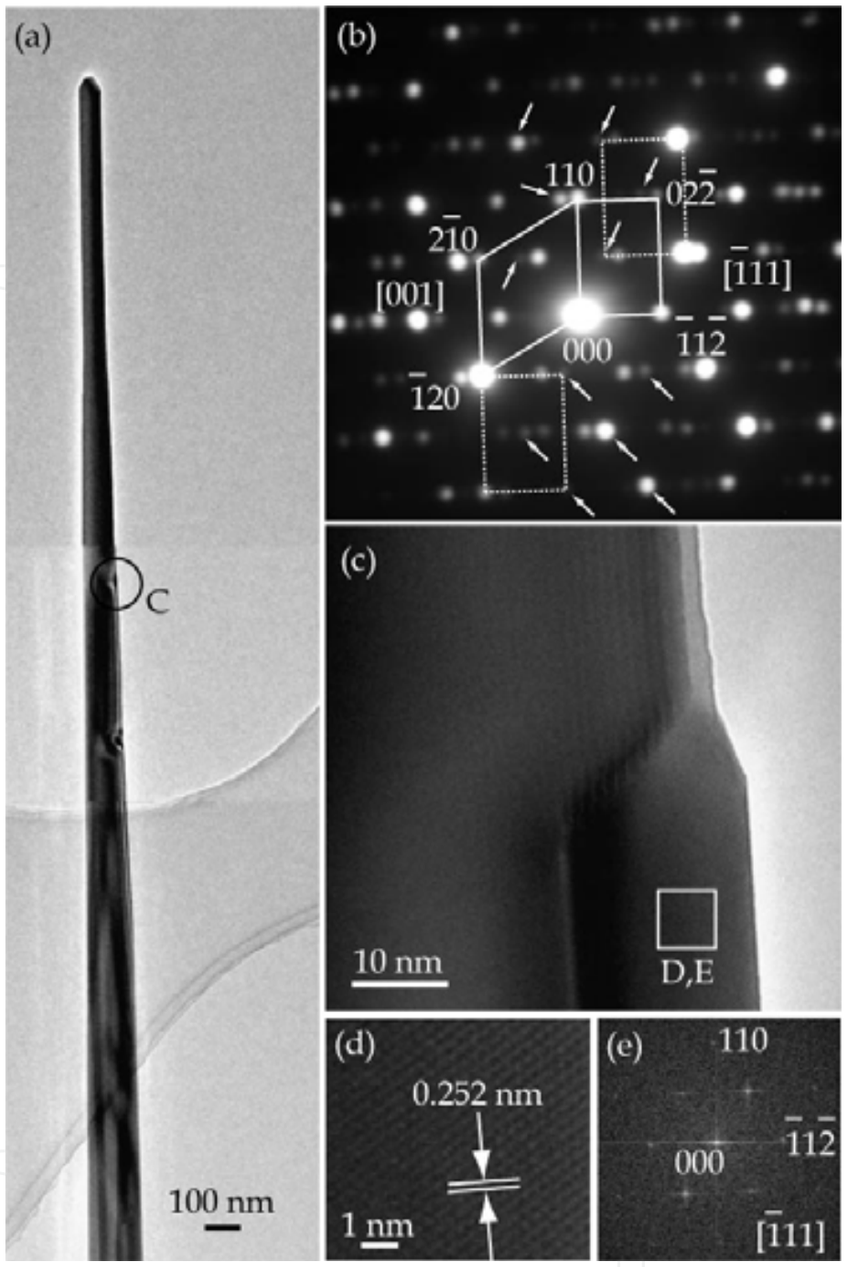

Fig. 10. (a) TEM image and (b) corresponding SAED pattern of one of the nanowires shown in Fig. 9 (a). (c) enlarged TEM image of the area marked by circle C in (a). (d) TEM image and (e) corresponding FFT pattern of the rectangular enclosed area in (c).

diameter of about 100 nm, is as small as that observed in Fig. 10 (a), but half as much as the width of the nanobelt. The SAED patterns reveal that either the nanobelt or the nanowire has a bicrystal structure with the growth direction along [110].

Figures 12 (a) and (e) show the TEM images of the nanobelts grown by the thermal oxidation of iron substrates at 800 ^{o}C (Fig. 9c). A nanobelt with a sharp tip is shown in Fig. 12 (a). Figures 12 (b-d) show the corresponding SAED patterns from the rectangular B, C and D enclosed areas in Fig. 12 (a), and Figures 12 (f-g) show the corresponding SAED

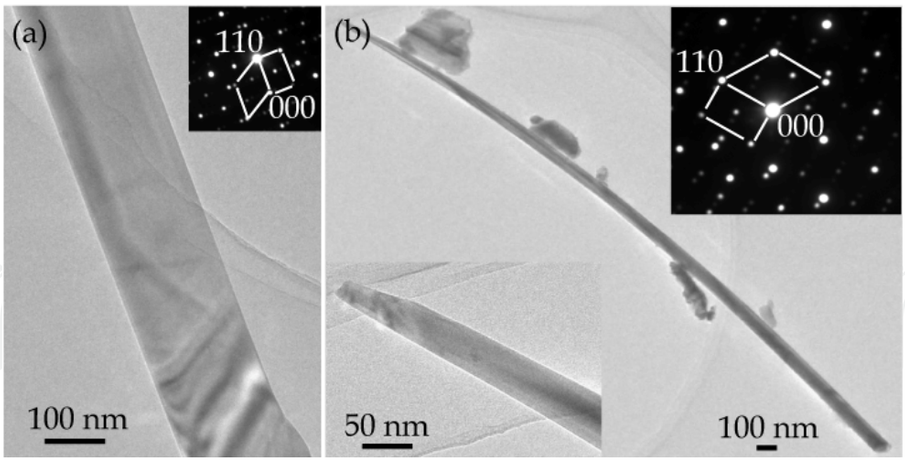

Fig. 11. (a) TEM image of the nanostructures shown in Fig. 9 (b). (b) TEM image of a nanobelt and corresponding SAED pattern in the inset. (c) TEM image of a nanowire with enlarged TEM image of the tip and corresponding SAED pattern in the insets, respectively.

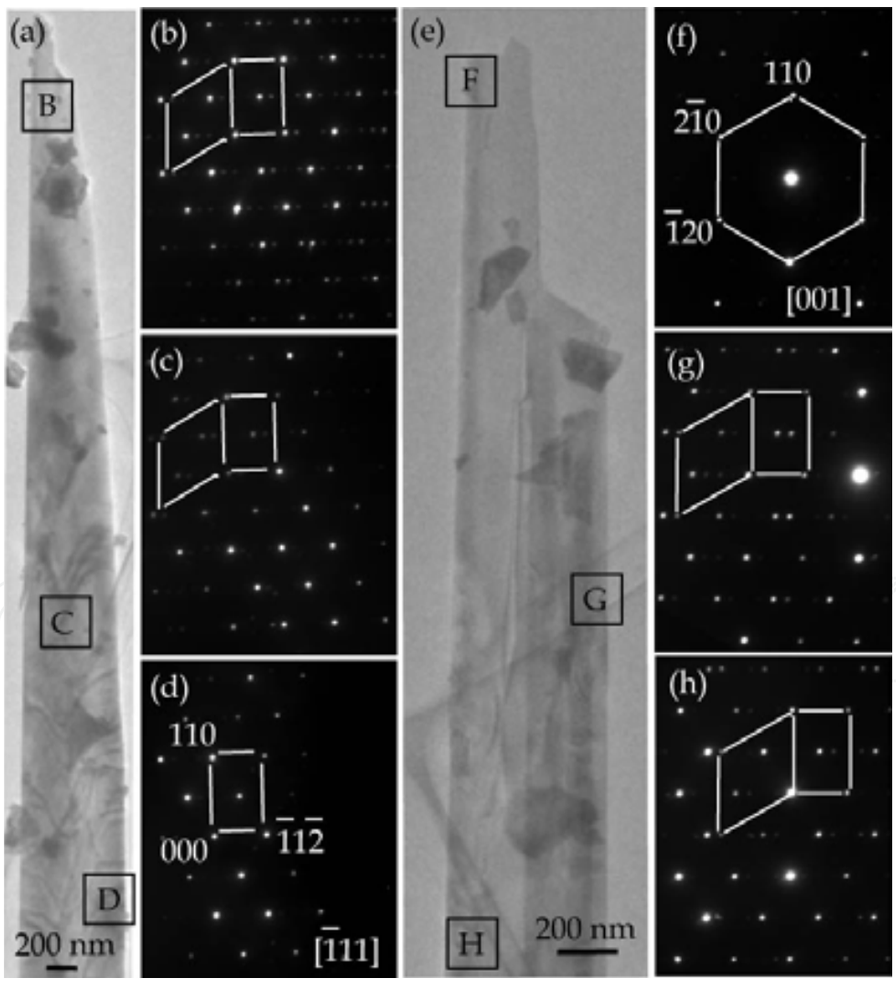

Fig. 12. (a,e) TEM images of the nanobelts shown in Fig. 9 (c). (b-d, f-h) corresponding SAED patterns recorded from rectangular D-E and F-H enclosed areas in (a) and (e), respectively.

patterns from the rectangular F, G and H enclosed areas in Fig. 12 (e). Although only one set of diffraction pattern is shown in Figs. 12 (d, f), actually some extra weak diffraction spots exist in the SAED patterns after careful examination. Thus, the nanobelts also have a bicrystal structure and grow along the [110] direction.

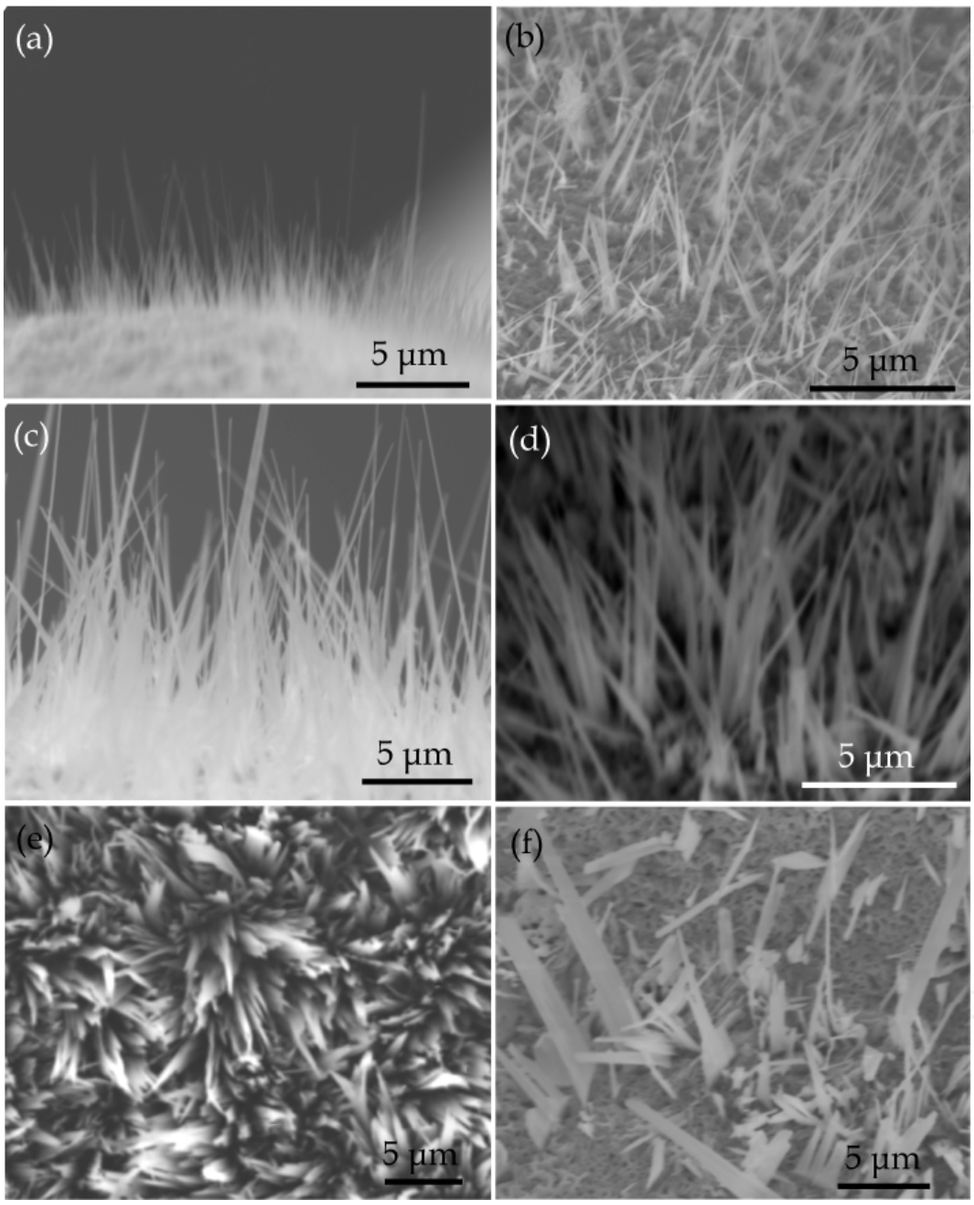

Fig. 13. SEM images of α-Fe_2O_3 nanostructures grown on iron substrates (a,c,e) without or (b,d,f) with gallium at (a,b) 600, (c,d) 650 and (e,f) 750 ^oC.

The surface energy is one of the major factors that affect the growth direction of the nanowire or nanobelt (Ye et al., 2005). The nanowires or nanobelts preferentially grow along the direction that minimizes their surface energy. Although the surface energy of the [110] orientation is not the highest (de Leeuw & Cooper, 2007), the α-Fe_2O_3 nanoscale crystals preferred to grow along the [110] direction (Cvelbar et al., 2008; Kim et al., 2006; Takagi,

1957). In the crystal structure of α-Fe_2O_3, the O atoms are close-packed in the (110) planes, the O-rich and Fe-deficient character on the (110) planes is considered to be the driving force for the preferential growth along the [110] direction (Srivastava et al., 2007; Wen et al., 2005). In addition, the bicrystal structure observed here did not affect the growth direction along [110].

In order to investigate the growth temperature dependence of the α-Fe_2O_3 nanostructure growth, the α-Fe_2O_3 nanostructure growth was tried by the thermal oxidation of iron substrates with or without gallium at temperatures of 600, 650 and 750 ^oC for 3 h in the air, as shown in Figure 13. By the thermal oxidation of iron substrates in the air, nanowires were grown at temperatures of 600~700 ^oC (Figs. 13a&c, 9a), while nanobelts were grown at temperatures of 750 (Fig. 13e) and 800 ^oC (Fig. 9c). The nanowires or nanobelts cover the surface of the irons and the density increases with the temperatures. However, nanobelts were grown by the thermal oxidation of iron substrates with gallium at temperatures of 600~750 ^oC, meanwhile, few nanowires were also observed (Figs. 13b,d&f, 9c). In addition, micro-crystals were grown at 800 ^oC, and nanostructures were seldom obtained (Fig. 9d). Most of the nanowires and nanobelts become narrow towards the tip, and the length extends to tens of micrometers. In addition, the nanowires are generally thinner than the nanobelts.

Due to the low Fe vapor pressure (Honig & Kramer, 1969), and no evidence of deposition was found anywhere except on the iron substrate, the evaporation can be negligible at the growth temperatures in the air. In consideration of the rough surface of the iron substrate as observed in the as-grown samples, it is assumed that nanoscale Fe droplets were formed on the surface of the iron substrate at elevated temperatures, and Fe and O were absorbed into the droplets from the iron substrate and the air, respectively. The α-Fe_2O_3 nanostructures would be formed on the iron surface when the droplets got supersaturated, and the growth would be terminated when the liquid is condensed into the solid state during cooling down (Kim et al., 2006; Yu et al., 2006). The α-Fe_2O_3 nanostructure growth should be controlled by the Fe surface diffusion and supersaturation (Lu & Ulrich, 2005; Takagi, 1957; Ye et al., 2005; Zhang et al., 2008).

In this study, the transformation from nanowire growth to nanobelt growth or even micro-crystal growth was observed in Figs. 9 and 13. It is generally suggested that high supersaturation favors the two-dimensional growth of the nanostructures (Lu & Ulrich, 2005; Ye et al., 2005; Zhang et al., 2008). At low temperatures (below 600 ^oC), few droplets were formed and the diffusion rate was very low, thus sparse nanowires were grown (Fig. 13a). More droplets were formed and the diffusion rate increased with the growth temperatures, thus the nanowires with high density were grown at 700 ^oC (Fig. 9a). When the temperature was higher than 750 ^oC (Figs. 13e&9c), the supersaturation was relatively high, two-dimensional nucleation would be initiated, and the increased diffusion rate accelerated the nanobelt growth (Wen et al., 2005). On the other hand, the presence of gallium would significantly decrease the formation temperature of the droplets by forming eutectic (Okamoto, 2000), and a high supersaturation could be achieved at low temperatures, which would facilitate the nanobelt growth, as compared with the nanowires grown by the thermal oxidization of iron. The nanobelts with a high density were grown at 700 ^oC (Fig. 9b), while micro-crystal growth rather than nanobelt growth occurred at 800 ^oC (Fig. 9d) due to the very high supersaturation and diffusion rate. In addition, the Fe diffusion from the bottom to tip is a diffusion limited process (Han et al., 2006), which is

considered to result in the narrowing of the nanowires (Figs. 10a&11c) and nanobelts towards the tip (Fig. 12a).

3.3 β-Ga_2O_3

β-Ga_2O_3 is chemically and thermally stable with a wide band-gap of 4.9 eV, thus has potential applications in optoelectronic devices (Fu et al., 2003) and high temperature stable gas sensors (Ogita et al., 1999). So far, a variety of β-Ga_2O_3 nanostructures has been widely synthesized through chemical vapor deposition (Zhang et al., 2008), thermal evaporation (Zhang et al., 1999) or catalytic assisted growth (Choi et al., 2009) using gallium as one of the starting materials. As comparison, β-Ga_2O_3 nanostructure growth was carried out by the thermal oxidation of gallium at temperatures of 700~900 °C for 24 h in air, and the β-Ga_2O_3 nanostructures were observed on the surface of molten gallium. As shown in Figure 14, a series of SEM images reveal the growth evolution with the increase in the growth temperatures. β-Ga_2O_3 nanowires with a length less than 1 μm were grown at 700 °C (Fig. 14a), while β-Ga_2O_3 nanowires with a high density were grown at 800 °C (Fig. 14b), and the density and length increased with the temperature (Fig. 14c). It is indicated that a high growth temperature favored the nucleation and nanowire growth of the β-Ga_2O_3 crystals.

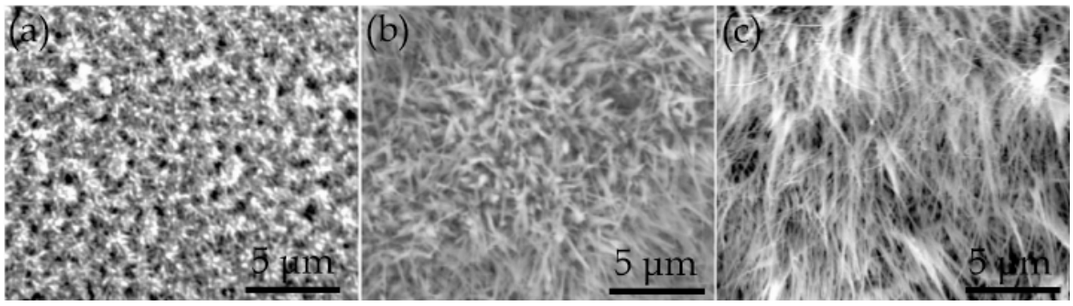

Fig. 14. SEM images of β-Ga_2O_3 nanowires grown at (a) 700, (b) 800 and (c) 900 °C.

4. Conclusion

In this study, we showed a variety of nanowire and nanobelt based oxides, including ZnO, α-Fe_2O_3 and β-Ga_2O_3, grown by the thermal oxidation with gallium in air. These results revealed the availability of such a simple growth method for the oxide nanostructure growth. In addition, the effect of gallium on the nanostructure growth (e.g., ZnO nanowires & nanobelts) and morphology transformation (e.g., α-Fe_2O_3 nanowires & nanobelts) was demonstrated, which provided the possibility of the selective growth of oxide nanostructures. Various other oxide nanostructures are expected when considering the anisotropic surface energy and nonhomogeneous supersaturation conditions, as well as the growth condition dependence of the selective growth.

5. References

Baxter, J. B.; Bessems, R. E. M. W. & Aydil, E. S. (2003). Growth and characterization of ZnO nanowires. *Materials Research Society Symposium Proceedings*, Vol.776, pp.Q7.9.1-Q7.9.6

Chen, J. T.; Zhang, F.; Wang, J.; Zhang, G. A.; Miao, B. B.; Fan, X. Y.; Yan, D. & Yan, P. X. (2008). CuO nanowires synthesized by thermal oxidation route. *Journal of Alloys and Compounds*, Vol.454, No.1-2, pp.268-273

Choi, K. H.; Cho, K. K.; Kim, K. W.; Cho, G. B.; Ahn, H. J. & Nam, T. H. (2009). Catalytic growth and structural characterization of semiconducting β-Ga_2O_3 nanowires. *Journal of Nanoscience and Nanotechnology*, Vol.9, No.6, pp.3728-3733

Cvelbar, U.; Chen, Z.; Sunkara, M. K. & Mozetic, M. (2008). Spontaneous growth of superstructure α-Fe_2O_3 nanowire and nanobelt arrays in reactive oxygen plasma. *Small*, Vol.4, No.10, pp.1610-1614

de Leeuw, N. H. & Cooper, T. G. (2007). Surface simulation studies of the hydration of white rust $Fe(OH)_2$, goethite α-FeO(OH) and hematite α-Fe_2O_3. *Geochimica et Cosmochimica Acta*, Vol.71, No.7, pp.1655-1673

Deng, G.; Ding, A.; Cheng, W.; Zheng, X. & Qiu, P. (2005). Two-dimensional zinc oxide nanostructure. *Solid State Communications*, Vol.134, No.4, pp.283-286

Ding, Y.; Gao, P. X. & Wang, Z. L. (2004). Catalyst-nanostructure interfacial lattice mismatch in determining the shape of VLS grown nanowires and nanobelts: a case of Sn/ZnO. *Journal of The American Chemical Society*, Vol.126, No.7, pp.2066-2072

Fu, L.; Liu, Y.; Hu, P.; Xiao, K.; Yu, G. & Zhu, D. (2003). Ga_2O_3 nanoribbons: synthesis, characterization, and electronic properties. *Chemistry of Materials*, Vol.15, No.22, pp.4287-4291

Fu, Y. Y.; Wang, R. M.; Xu, J.; Chen, J.; Yan, Y.; Narlikar, A. V. and Zhang, H. (2003). Synthesis of large arrays of aligned α-Fe_2O_3 nanowires. *Chemical Physics Letters*, Vol.379, No.3-4, pp.373-379

Gu, G.; Zheng, B.; Han, W. Q.; Roth, S. & Liu, J. (2002). Tungsten oxide nanowires on tungsten substrates. *Nano Letters*, Vol.2, No.8, pp.849-851

Han, Q.; Xu, Y. Y.; Fu, Y. Y.; Zhang, H.; Wang, R. M.; Wang, T. M. & Chen, Z. Y. (2006). Defects and growing mechanisms of α-Fe_2O_3 nanowires. *Chemical Physics Letters*, Vol.431, No.1-3, pp.100-103

Honig, R. E. & Kramer, D. A. (1969). Vapor pressure data for the solid and liquid elements. *RCA Review*, Vol.30, pp.285-305

Hu, J. Q.; Ma, X. L.; Xie, Z. Y.; Wong, N. B.; Lee, C. S. & Lee, S. T. (2001). Characterization of zinc oxide crystal whiskers grown by thermal evaporation. *Chemical Physics Letters*, Vol.344, No.1-2, pp.97-100

Jian, J. K.; Wang, C.; Zhang, Z. H.; Chen, X. L.; Xu, L. H. & Wang, T. M. (2006). Necktie-like ZnO nanobelts grown by a self-catalytic VLS process. *Materials Letters*, Vol.60, No.29-30, pp.3809-3812

Jiang, X.; Herricks, T. & Xia, Y. (2002). CuO nanowires can be synthesized by heating copper substrates in air. *Nano Letters*, Vol.2, No.12, pp.1333-1338

Kim, C. H.; Chun, H. J.; Kim, D. S.; Kim, S. Y.; Park, J.; Moon, J. Y.; Lee, G.; Yoon, J.; Jo, Y.; Jung, M. H.; Jung, S. I. & Lee, C. J. (2006). Magnetic anisotropy of vertically aligned α-Fe_2O_3 nanowire array. *Applied Physics Letters*, Vol.89, No.22, pp.223103

Kubaschewski, O. & Alcock, C. B. (1979). *International Series on Materials Science and Technology: Metallurgical Thermo-Chemistry*, Pergamon Press, Oxford

Li, W. J.; Shi, E. W.; Zhong, W. Z. & Yin, Z. W. (1999). Growth mechanism and growth habit of oxide crystals. *Journal of Crystal Growth*, Vol.203, No.1-2, pp.186-196

Li, Y.; You, L.; Duan, R.; Shi, P. & Qin, G. (2004). Oxidation of a ZnS nanobelt into a ZnO nanotwin belt or double single-crystalline ZnO nanobelts. *Solid State Communications*, Vol.129, No.4, pp.233-238

Liao, L.; Zheng, Z.; Yan, B.; Zhang, J. X.; Gong, H.; Li, J. C.; Liu, C.; Shen, Z. X. & Yu, T. (2008). Morphology controllable synthesis of α-Fe_2O_3 1D nanostructures: growth mechanism and nanodevice based on single nanowire. *The Journal of Physical Chemistry C*, Vol.112, No.29, pp.10784-10788

Lu, J. G.; Chang, P. & Fan, Z. (2006). Quasi-one-dimensional metal oxide materials - synthesis, properties and applications. *Materials Science and Engineering R*, Vol.52, No.1-3, pp.49-91

Lu, J. J. & Ulrich, J. (2005). The influence of supersaturation on crystal morphology - experimental and theoretical study. *Crystal Research and Technology*, Vol.40, No.9, pp.839-846

Majni, G.; Nobili, C.; Ottaviani, G.; Costaato, M. & Galli, E. (1981). Gold-aluminum thin-film interactions and compound formation. *Journal of Applied Physics*, Vol.52, No.6, pp.4047-4054

Miyake, A.; Kominami, H.; Tatsuoka, H.; Kuwabara, H.; Nakanishi, Y. & Hatanaka, Y. (2000). Growth of epitaxial ZnO thin film by oxidation of epitaxial ZnS film on Si(111) substrate. *Japanese Journal of Applied Physics*, Vol.39, No.11B, pp.L1186-L1187

Ogino, K.; Honda, S.; Yasuda, T.; Tatsuoka, H.; Inaba, T.; Kominami, H.; Nakanishi, Y. & Murakami, K. (2007). Simple synthesis of a variety of nano-structures using silicide alloys with Ga droplets. *ECS Transactions*, Vol.11, No.8, pp.77-81

Ogita, M.; Saika, N.; Nakanishi, Y. & Hatanaka, Y. (1999). Ga_2O_3 thin films for high-temperature gas sensors. *Applied Surface Science*, Vol.142, No.1-4, pp.188-191

Ohmori, T.; Takahashi, H.; Mametsuka, H. & Suzuki, E. (2000). Photocatalytic oxygen evolution on α-Fe_2O_3 films using Fe^{3+} ion as a sacrificial oxidizing agent. *Physical Chemistry Chemical Physics*, Vol.2, No.14, pp.3519-3522

Okamoto, H. (2000). *in Desk Handbook: Phase Diagrams for Binary Alloys*, ASM International, Materials Park, OH

Pan, Z. W.; Dai, Z. R. & Wang, Z. L. (2001). Nanobelts of semiconducting oxides. *Science*, Vol.291. No.5510, pp.1947-1949

Pan, Z. W.; Dai, Z. R.; Ma, C. & Wang, Z. L. (2002). Molten gallium as a catalyst for the large-scale growth of highly aligned silica nanowires. *Journal of the American Chemical Society*, Vol.124, No.8, pp.1817-1822

Pan, Z. W.; Dai, S.; Beach, D. B. & Lowndes, D. H. (2003). Temperature dependence of morphologies of aligned silicon oxide nanowire assemblies catalyzed by molten gallium. *Nano Letters*, Vol.3, No.9, pp.1279-1284

Pan, Z. W.; Dai, S. & Lowndes, D. H. (2005). Gallium-catalyzed silicon oxide nanowire growth. *Tsinghua Science and Technology*, Vol.10, No.6, pp.718-728

Ren, S.; Bai, Y. F.; Chen, J.; Deng, S. Z.; Xu, N. S.; Wu, Q. B. & Yang, S. (2007). Catalyst-free synthesis of ZnO nanowire arrays on zinc substrate by low temperature thermal oxidation. *Materials Letters*, Vol.61, No.3, pp.666-670

Srivastava, H.; Tiwari, P.; Srivastava, A. K. & Nandedkar, R. V. (2007). Growth and characterization of α-Fe_2O_3 nanowires. *Journal of Applied Physics*, Vol.102, No.5, pp.054303

Takagi, R. (1957). Growth of oxide whiskers on metals at high temperature. *Journal of The Physical Society of Japan*, Vol.12, No.11, pp.1212-1218

Wang, G. Z.; Ma, N. G.; Deng, C. J.; Yu, P.; To, C. Y.; Hung, N. C.; Aravind, M. & Dickon H. L. Ng (2004). Large-scale synthesis of aligned hexagonal ZnO nanorods using chemical vapor deposition. *Materials Letters*, Vol.58, No.16, pp.2195-2198

Wang, R.; Chen, Y.; Fu, Y.; Zhang, H. & Kisielowski, C. (2005). Bicrystalline hematite nanowires. *The Journal of Physical Chemistry B*, Vol.109, No.25, pp.12245-12249

Wang, X.; Ding, Y.; Summers, C. J. & Wang, Z. L. (2004). Large-scale synthesis of six-nanometer-wide ZnO nanobelts. *The Journal of Physical Chemistry B*, Vol.108, No.26, pp.8773-8777

Wen, X.; Wang, S.; Ding, Y.; Wang, Z. L. & Yang, S. (2005). Controlled growth of large-area, uniform, vertically aligned arrays of α-Fe_2O_3 nanobelts and nanowires. *The Journal of Physical Chemistry B*, Vol.109, No.1, pp.215-220

Xu, Y. Y.; Zhao, D.; Zhang, X. J.; Jin, W. T.; Kashkarov, P. & Zhang, H. (2009). Synthesis and characterization of single-crystalline α-Fe_2O_3 nanoleaves. *Physica E*, Vol.41, No.5, pp.806-811

Yang, Q.; Tanaka, M.; Yasuda, T. & Tatsuoka, H. (2009). Growth of ZnO nanowires using ZnS substrates with Ga droplets. *e-Journal of Surface Science and Nanotechnology*, Vol. 7, pp.25-28

Ye, C.; Fang, X.; Hao, Y.; Teng, X. & Zhang, L. (2005). Zinc oxide nanostructures: morphology derivation and evolution. *The Journal of Physical Chemistry B*, Vol.109, No.42, pp.19758-19765

Yu, T.; Zhu, Y.; Xu, X.; Shen, Z.; Chen, P.; Lim, C. T.; Thong, J. T. L. & Sow, C. H. (2005). Controlled growth and field-emission properties of cobalt oxide Nanowalls. *Advanced Materials*, Vol.17, No.13, pp.1595-1599

Yu, T.; Zhu, Y.; Xu, X.; Yeong, K. S.; Shen, Z.; Chen, P.; Lim, C. T.; Thong, J. T. L. & Sow, C. H. (2006). Substrate-friendly synthesis of metal oxide nanostructures using a hotplate. *Small*, Vol.2, No.1, pp.80-84

Yuan, H. J.; Xie, S. S.; Liu, D. F.; Yan, X. Q.; Zhou, Z. P.; Ci, L. J.; Wang, J. X.; Gao, Y.; Song, L.; Liu, L. F.; Zhou, W. Y. & Wang, G. (2003). Characterization of zinc oxide crystal nanowires grown by thermal evaporation of ZnS powders. *Chemical Physics Letters*, Vol.371, No.3-4, pp.337-341

Zhang, H. Z.; Kong, Y. C.; Wang, Y. Z.; Du, X.; Bai, Z. G.; Wang, J. J.; Yu, D. P.; Ding, Y.; Hang, Q. L. & Feng, S. Q. (1999). Ga_2O_3 nanowires prepared by physical evaporation. *Solid State Communications*, Vol.109, No.11, pp.677–682

Zhang, X.; Liu, Z. & Hark, S. (2008). Synthesis and cathodoluminescence of β-Ga_2O_3 nanowires with holes. *Journal of Nanoscience and Nanotechnology*, Vol.8, No.3, pp.1284-1287

Zhang, Y.; Li, R.; Zhou, X.; Cai, M. & Sun, X. (2008). Selective growth of α-Al_2O_3 nanowires and nanobelts. *Journal of Nanomaterials*, Vol.2008, pp.250370

Zhao, D.; Andreazza, C.; Andreazza, P.; Ma, J.; Liu, Y. & Shen, D. (2004). Temperature-dependent growth mode and photoluminescence properties of ZnO nanostructures. *Chemical Physics Letters*, Vol.399, No.4-6, pp.522-526

Nanowires Science and Technology

Edited by Nicoleta Lupu

ISBN 978-953-7619-89-3
Hard cover, 402 pages
Publisher InTech
Published online 01, February, 2010
Published in print edition February, 2010

This book describes nanowires fabrication and their potential applications, both as standing alone or complementing carbon nanotubes and polymers. Understanding the design and working principles of nanowires described here, requires a multidisciplinary background of physics, chemistry, materials science, electrical and optoelectronics engineering, bioengineering, etc. This book is organized in eighteen chapters. In the first chapters, some considerations concerning the preparation of metallic and semiconductor nanowires are presented. Then, combinations of nanowires and carbon nanotubes are described and their properties connected with possible applications. After that, some polymer nanowires single or complementing metallic nanowires are reported. A new family of nanowires, the photoferroelectric ones, is presented in connection with their possible applications in non-volatile memory devices. Finally, some applications of nanowires in Magnetic Resonance Imaging, photoluminescence, light sensing and field-effect transistors are described. The book offers new insights, solutions and ideas for the design of efficient nanowires and applications. While not pretending to be comprehensive, its wide coverage might be appropriate not only for researchers but also for experienced technical professionals.

INTECH
open science | open minds

InTech Europe
University Campus STeP Ri
Slavka Krautzeka 83/A
51000 Rijeka, Croatia
Phone: +385 (51) 770 447
Fax: +385 (51) 686 166
www.intechopen.com

InTech China
Unit 405, Office Block, Hotel Equatorial Shanghai
No.65, Yan An Road (West), Shanghai, 200040, China
中国上海市延安西路65号上海国际贵都大饭店办公楼405单元
Phone: +86-21-62489820
Fax: +86-21-62489821

IntechOpen